

# Efficient Octave-Spanning Parametric Down-Conversion at the Picojoule Level

Marc Jankowski\*,<sup>1,2,\*</sup> Nayara Jornod\*,<sup>1</sup> Carsten Langrock,<sup>1</sup> Boris Desiatov,<sup>3</sup> Alireza Marandi,<sup>4</sup> Marko Lončar,<sup>3</sup> and Martin M. Fejer<sup>1</sup>

<sup>1</sup>*Edward L. Ginzton Laboratory, Stanford University, Stanford, California 94305, USA*

<sup>2</sup>*NTT Research Inc. Physics and Informatics Labs, 940 Stewart Drive, Sunnyvale, California*

<sup>3</sup>*John A. Paulson School of Engineering and Applied Sciences, Harvard University, Cambridge, Massachusetts 02138, USA*

<sup>4</sup>*Department of Electrical Engineering, California Institute of Technology, Pasadena, California 91125, USA*

(Dated: June 9, 2022)

The generation and amplification of photons by parametric down-conversion in quadratic nonlinear media is used as a source of entangled photons, squeezed light, and short optical pulses at difficult to access wavelengths. Optical nonlinearities are inherently weak, and therefore the pump energy required to produce sufficient gain for efficient down-conversion has been limited to energies in excess of nanojoules [1]. Here we use dispersion-engineered nonlinear nanowaveguides driven by femtosecond pulses to demonstrate efficient down-conversion at the picojoule level; we observe parametric gains in excess of 70 decibels with pump pulse energies as little as 4 picojoules. When driven with pulse energies in excess of 10 picojoules these waveguides amplify vacuum fluctuations to >10% of the pump power, and the generated bandwidth broadens to span an octave. These results represent a new class of parametric devices that combine sub-wavelength spatial confinement with femtosecond pulses to achieve efficient operation with remarkably low energy.

Parametric down-conversion (PDC) in quadratic ( $\chi^{(2)}$ ) nonlinear media is an indispensable process in both quantum and classical nonlinear optics. In this process, a short wavelength pump provides gain to photons at longer wavelengths. In the absence of a coherent seed this process amplifies vacuum fluctuations to produce photon pairs and squeezed light. When seeded by a coherent signal or embedded in a resonator, PDC produces broadband coherent light at otherwise hard to access wavelengths and is an essential tool in spectroscopy. In almost every application both large parametric gains and low-energy operation are desirable.

The energy required for PDC has historically been limited by trade-offs between the interaction length of a device and the intensity of the focused light. For tightly focused Gaussian beams in bulk nonlinear media the intensity of the field is limited either by the spatial walk-off or diffraction (Fig. 1(a)). Spatial walk-off dominates in devices based on birefringent phasematching, while diffraction dominates for confocally-focused beams in devices based on quasi-phasematching (QPM). An analogous set

of trade-offs occur when these processes are driven by femtosecond pulses (Fig. 1(b)). The pulse duration, and therefore the peak intensity available for a nonlinear interaction, is limited either by temporal walk-off or by pulse spreading due to the dispersion of the interacting waves. As a benchmark we consider optical parametric generation (OPG), where PDC is driven with enough gain to amplify vacuum fluctuations to macroscopic intensities. Typical devices based on quasi-phasematching in bulk media operate with 10's or 100's of nanojoules of pulse energy due to the interplay of these constraints (Fig. 1(c)). State-of-the-art devices based on QPM in diffused waveguides eliminate both spatial walk-off and diffraction, and achieve efficiencies as large as 33% when driven by nanojoules [1].

This work builds on recent progress in periodically poled thin-film lithium niobate (TFLN) nanophotonics to demonstrate efficient OPG of a broadband signal at 2  $\mu\text{m}$  using only picojoules of pump pulse energy. The TFLN waveguides used here have several key advantages over previous approaches: i) the sub-wavelength confinement in nanophotonic waveguides enhances the field intensity of the interacting modes 20-fold relative to diffused waveguides [20, 21], and ii) the geometry dependence of the dispersion associated with the pump and signal can be used to engineer the interaction lengths of short pulses. We use the dispersion engineering available in nanophotonic waveguides to achieve quasi-static operation by simultaneously eliminating both temporal walk-off between the pump and signal, and pulse spreading due to group velocity dispersion (GVD) of the signal. This allows a 6-millimeter-long waveguide to be driven with pulse durations of 80 femtoseconds and provide parametric gain across a micron of bandwidth. The resulting devices operate with remarkably low energies. We observe OPG with as little as 60 femtojoules of pump energy. When driven with pulse energies in excess of 10 picojoules these waveguides exhibit a saturated gain as large as 88 dB, corresponding to a conversion efficiency of 10%. In the saturated regime, the generated signal broadens to span an octave of bandwidth.

When operated near degeneracy, parametric downconversion of short pulses is dominated by two dispersion orders: the group velocity mismatch  $\Delta k' = k'_{2\omega} - k'_{\omega}$  between the pump at  $2\omega$  and the generated signal centered around  $\omega$ , and the GVD of the signal  $k''_{\omega}$ . The

\* These authors contributed equally. marcjank@stanford.edu

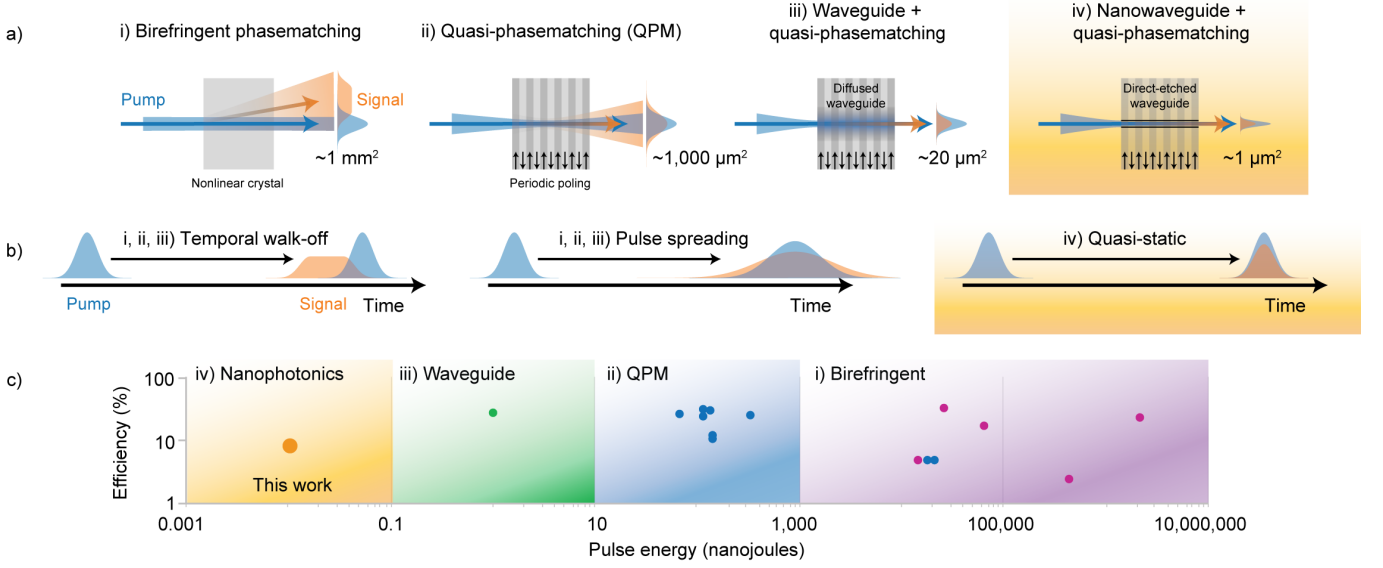


FIG. 1. **The route towards efficient low-energy nonlinear interactions.** **a**, Successive generations of nonlinear devices have relied on improving the spatial confinement of the interacting waves to reduce the energy required for efficient parametric down-conversion. The effective areas listed here correspond to OPG of  $2\ \mu\text{m}$  light in a 1-cm-long crystal of lithium niobate. In the case of nanophotonic devices, the fields may be confined to a wavelength  $(\lambda/n)^2$ . **b**, A similar reduction of the energy requirements is enabled by using short pulses. Here, the minimum pulse duration, and therefore the peak intensity, is limited by a combination of temporal walk-off and pulse spreading during the propagation. Nanophotonic devices may achieve quasi-static operation by eliminating both of these effects through dispersion engineering. These devices enable arbitrarily long interactions of short pulses confined in a sub-wavelength device. **c**, When compared to previous demonstrations of optical parametric generation [1–19], quasi-static nanophotonic devices operate with orders of magnitude less energy.

group velocity mismatch between the interacting harmonics in a nonlinear device  $\Delta k'$  limits the pump bandwidth available for PDC, and therefore sets a minimum usable pump pulse duration. Similarly, the GVD per gain length of the fundamental  $k''_{\omega}/\gamma_{\text{pk}}$  limits the amount of bandwidth around  $\omega$  that can be generated by PDC. Here,  $\gamma_{\text{pk}} = \kappa\sqrt{P_{\text{pk}}}$  is the unsaturated gain coefficient given by the peak power of the pump pulse  $P_{\text{pk}}$ , and  $\kappa$  is the nonlinear coupling (see methods). In the absence of these effects, the amount of pump bandwidth that can contribute to PDC is dominated by GVD ( $k''_{\omega}$ ), and the generated signal bandwidth is dominated by fourth-order dispersion ( $k''_{\omega}^{(4)}$ ). Recent work has shown that both temporal walk-off and GVD of the signal can be simultaneously eliminated using geometric dispersion in a TFLN nanowaveguide [21], and demonstrated efficient second-harmonic generation (SHG) of short pulses. We adopt the same approach for OPG here.

Figure 2 summarizes the relevant design parameters of a nanophotonic waveguide designed for broadband PDC driven by short pulses centered around 1045 nm. We use 6-mm-long waveguides fabricated in a 700-nm-thick lithium niobate film (NANOLN) having a top width of 1850 nm and an etch depth of 340 nm (Fig. 2a). The resulting  $\Delta k'$  and  $k''_{\omega}$  are shown in Fig. 2b and c, respectively, showing  $\Delta k' \sim 5\ \text{fs/mm}$ ,  $k''_{\omega} \sim 6\ \text{fs}^2/\text{mm}$ , and  $k''_{2\omega} \sim 80\ \text{fs}^2/\text{mm}$ . For the propagation lengths considered here and the 80-fs pulse duration of the pump,

both temporal walk-off and pump dispersion are negligible, and the entire pump bandwidth may contribute to PDC. Furthermore, in the absence of GVD around the signal we expect the generated signal bandwidth to drastically exceed the input pump bandwidth. Under these conditions, the power gain experienced by a signal at frequency  $\omega + \Omega'$  can be approximated as (see methods)

$$P_{\omega}(z, \Omega') \approx P_{\omega}(0, \Omega') \exp(2g(\Omega')z), \quad (1)$$

where  $g(\Omega') = \sqrt{\gamma_{\text{pk}}^2 - (\Delta k_{\omega}(\Omega')/2)^2}$  is the field gain coefficient. The frequency dependent phase-mismatch is given by  $\Delta k_{\omega}(\Omega') \approx k_{2\omega}(2\omega) - k_{\omega}(\omega + \Omega') - k_{\omega}(\omega - \Omega') - 2\pi/\Lambda_G$ , where  $\Lambda_G$  is the period of the QPM grating. Exponential growth occurs for frequencies around  $\Delta k_{\omega}(\Omega') = 0$ , with oscillatory solutions occurring for  $\Omega'$  where  $\Delta k_{\omega}(\Omega') > 2\gamma_{\text{pk}}$ . Figure 2d shows the calculated gain available for OPG as a function of the phase-mismatch between the pump and signal,  $\Delta k_{\omega}(0)$ , and the wavelength of the generated signal. Here we assume a pump pulse energy of 1 pJ, and a pulse duration of 80 fs. When the fundamental and second harmonic are close to phase-matching, the calculated gain spectrum exceeds 50 dB across nearly a micron of bandwidth ( $\sim 1700 - 2600\ \text{nm}$ ). We note here that a slight offset of the phase-mismatch ( $\Delta k = 1 - 2.5\ \text{mm}^{-1}$ ) can enhance the gain bandwidth by hundreds of nanometers [22].

We characterize these waveguides using the experimen-

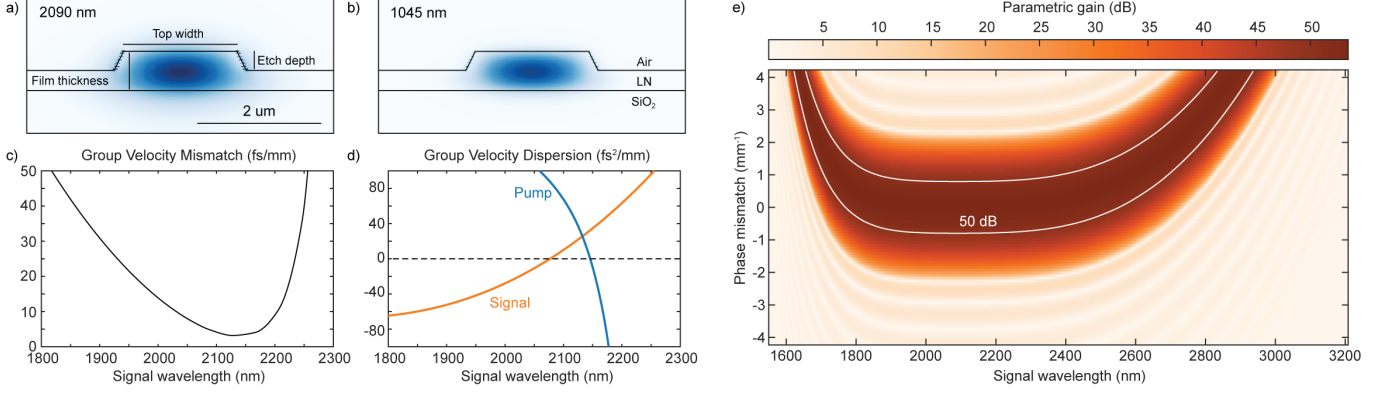


FIG. 2. **Design of the dispersion engineered waveguide.** **a,b**, Waveguide cross-section and the normalized electric field of simulated TE<sub>00</sub> **a**) signal and **b**) pump. **c**, Simulated group velocity mismatch ( $\Delta k'$ ), and **d**, and group velocity dispersion ( $\Delta k''$ ). **e**, Simulated OPG bandwidth for a pump pulse energy of 1 pJ. Solid white contour lines correspond to 50 dB of gain.

tal setup presented in Fig. 3 (a). 80-fs pulses from a laser emitting at 1047 nm with a repetition frequency of 100 MHz (Menlo Systems Orange A) are coupled into the waveguide using a reflective objective lens (Thorlabs LMM-40X-P01). A similar objective is placed at the output to collect the generated signal and transmitted pump for characterization. The waveguide considered here was operated with a phase-mismatch of  $1.5\text{--}2\text{ mm}^{-1}$  to produce OPG from 1650 to 2800 nm.

We observe the onset of OPG with only 60 fJ of input pulse energy, limited by the noise floor of our photoreceiver and the 1-s integration time used for lock-in detection. The conversion efficiency of the parametric fluorescence and the depletion of the input pump as a function of the input pulse energy are presented in Fig. 3b. At low power we observe the expected  $\sqrt{P_{\text{in}}}$  dependence of the exponential growth on the logarithmic scale (inset), and find a fitted gain coefficient of  $35.5\text{ dB}/\sqrt{\text{pJ}}$  (black line), in reasonable agreement with the  $50\text{ dB}/\sqrt{\text{pJ}}$  predicted by quasi-static theory. This observed deviation between theory and experiment may be due to either nonidealities in periodic poling, such as shallow domain depths, or coupling of the pump to higher order spatial modes at the input, which would reduce the amount of pump power available for PDC. For pulse energies larger than 4 pJ, the pump exhibits a depletion in excess of 10%, and the signal gain begins to fall below the exponential fit used here. At a pump pulse energy of 4 pJ we find a power gain of 71 dB, or 118 dB/cm. The conversion efficiency then reaches a plateau of 11% for pump pulse energies above 10 pJ. For a pump energy of 18 pJ we measured a signal power of  $200\text{ }\mu\text{W}$  (2 pJ), which corresponds to a saturated gain of 88 dB.

The observed pump depletion ( $>60\%$ ) drastically exceeds the measured fractional power of the second harmonic (11%). We attribute this to parasitic SHG of the pump light. For all levels of pumping we observe green light scattering out of the waveguide, with a small frac-

tion collected by the output objective. This scattering is due to a combination of surface roughness and lateral leakage into slab modes, the latter of which becomes more pronounced at short wavelengths [23]. The right axis of Fig. 3b shows the collected green power due to parasitic SHG measured at the output of the waveguide. To better quantify the generated green, we repeated these measurements for both a narrower waveguide and an identical waveguide with a larger phase-mismatch. Neither of these waveguides produced measurable  $2\text{-}\mu\text{m}$  signals, and in both cases the observed pump depletion was comparable to the pump depletion observed here. We therefore expect the pump depletion due to parasitic SHG to be sufficiently large to be detrimental to the PDC efficiency.

The experimentally measured spectrum is presented in Fig. 3c. At input energies below 5 pJ we observe the formation of a broadband signal spanning from 1700 nm to 2700 nm (70 THz), in good agreement with the expected OPA bandwidth. When the pump energy is increased beyond 5 pJ, the signal partially depletes the pump and both are observed to undergo spectral broadening. For pulse energies in excess of 7 pJ, the pump and signal merge into a broadband spectrum. The dips in the spectrum around 2750 nm and 2850 nm are due to OH-absorption in the silica substrate and lithium niobate, respectively, and can be reduced by annealing the bulk materials before fabricating the thin films [24]. Any light generated beyond 2900 nm is absorbed in the silica and not observed here. We note here that spectral broadening of the pump is also observed in waveguides that do not exhibit PDC, and we therefore attribute this broadening to self-phase modulation.

While the gain and bandwidth generated by OPG at low power agree well with the behavior expected from theory, the observed behavior at high power includes spectral broadening of the signal and pump, as well as pump depletion due to parasitic SHG. To better understand the interplay of each of these mechanisms, we sim-

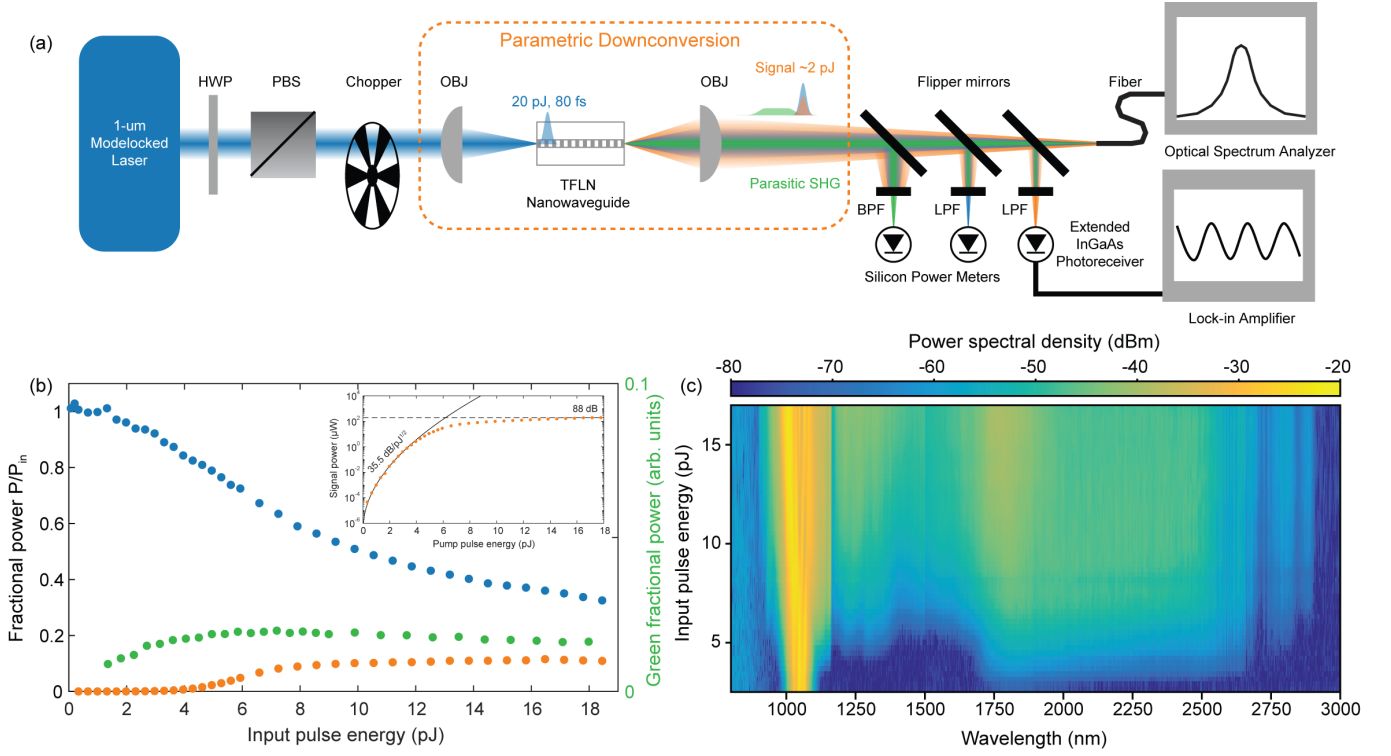


FIG. 3. **Characterization of OPG in TFLN nanowaveguides.** **a**, Experimental setup. HWP, half-wave plate; PBS, polarizing beamsplitter; OBJ, reflective objective lens; LPF, long pass filter; BPF, band pass filter. **b**, Left axis: OPG efficiency (orange), and pump depletion (blue) as a function of input pulse energy; Right axis: Parasitic green conversion efficiency, in arbitrary units. Inset: Logarithmic scale of the generated signal power at low pump energy and a square root curve fitting the data, showing a gain of  $35.5 \text{ dB}/\sqrt{\text{pJ}}$ . **c**, Generated spectrum as a function of input pulse energy.

ulate the evolution of the interacting waves using an adaptive split-step Fourier method that includes three envelopes in the equations of motion: the fundamental around  $2 \mu\text{m}$ , the pump around  $1 \mu\text{m}$ , and parasitic green light formed by second-harmonic generation (SHG) of the pump around  $520 \text{ nm}$ . The multi-envelope approach used here allows us to develop intuition about the various interacting nonlinear processes by isolating each of the relevant nonlinear interactions [25].

Figure 4 shows a comparison of the measured (black) and simulated (light green) spectra for a selection of pump pulse energies, showing qualitative agreement between simulation and experiment. To isolate the role of each nonlinear interaction, we repeat these simulations in the absence of the nonlinear polarization generated by the interaction in question. The evolution of the generated harmonics is unchanged in the absence of a  $\chi^{(3)}$  nonlinearity, and therefore the observed spectral broadening of the pump and signal is dominated by quadratic nonlinearities. We neglect third order nonlinearities in any further discussion. In the absence of coupling between the pump and the signal we still observe both depletion and spectral broadening of the pump, and we therefore attribute this spectral broadening to back-action by the parasitic green. This cascaded  $\chi^{(2)}$  process contributes a large negative effective self-phase modulation, which

causes the pump pulses to compress in the presence of normal dispersion, thereby broadening the optical spectrum. Finally, in the absence of coupling between the pump and the parasitic green we still observe spectral broadening of the generated  $2\text{-}\mu\text{m}$  signal. Therefore, we attribute this broadening to pump depletion and back-conversion of the generated signal. This process also broadens the pump, and therefore the spectral broadening presented here has contributions from both pump depletion and parasitic SHG. We note here that in the absence of parasitic SHG these simulations suggest that the conversion efficiency can be as large as 50%. In the presence of parasitic SHG, the generated signal power clamps at  $\sim 25\%$ , which suggests that parasitic SHG limits the generated signal power.

In summary, we have presented efficient parametric down-conversion across an octave of bandwidth with only picojoules of pulse energy. This low energy operation was made possible by a new generation of dispersion-engineered  $\chi^{(2)}$  nonlinear nanophotonic waveguides. The nanowaveguides used here achieve sub-wavelength spatial confinement of the interacting waves and use dispersion engineering to simultaneously eliminate temporal walk-off and pulse spreading. The resulting field intensities and interaction lengths for femtosecond pulses exceed previous approaches by more than an order of

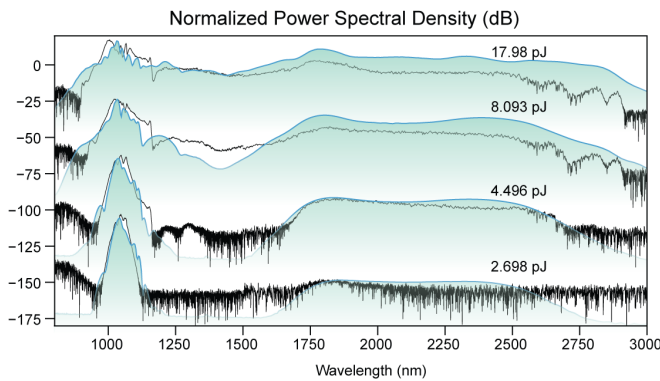


FIG. 4. **Selection of measured power spectral density compared with simulations.** Adjacent traces are shifted by 40 dB to facilitate readability. Light green: simulation

magnitude, thereby enabling a new class of efficient parametric devices that operate with orders of magnitude less energy than previous results. We have discussed two main limitations of the process: i) the reduced conversion efficiency due to the parasitic green light generated by SHG of the pump, and ii) the attenuation of the generated spectrum at wavelengths beyond 2900 nm due to absorption in the silica substrate. Longer wavelength operation can become possible by using mid-infrared compatible substrates, such as lithium niobate on sapphire [26]. Similarly, these parasitic loss mechanisms may be suppressed by engineering the QPM grating. [27]. We believe that dispersion-engineered quasi-phasematched nanowaveguides such as those shown here represent a crucial step towards compact parametric devices that operate with exceptionally low power.

- [1] X. Xie, A. M. Schober, C. Langrock, R. V. Roussev, J. R. Kurz, and M. M. Fejer, *J. Opt. Soc. Am. B* **21**, 1397 (2004), URL <http://josab.osa.org/abstract.cfm?URI=josab-21-7-1397>.
- [2] P. S. Kuo, K. L. Vodopyanov, M. M. Fejer, D. M. Simanovskii, X. Yu, J. S. Harris, D. Bliss, and D. Weyburne, *Opt. Lett.* **31**, 71 (2006), URL <http://ol.osa.org/abstract.cfm?URI=ol-31-1-71>.
- [3] M. Levenius, V. Pasiskevicius, F. Laurell, and K. Gallo, *Opt. Express* **19**, 4121 (2011), URL <http://www.opticsexpress.org/abstract.cfm?URI=oe-19-5-4121>.
- [4] O. Prakash, H.-H. Lim, B.-J. Kim, K. Pandiyan, M. Cha, and B. K. Rhee, *Appl. Phys. B* **92**, 535 (2008).
- [5] M. Tiihonen, V. Pasiskevicius, A. Fragemann, C. Canalias, and F. Laurell, *Appl. Phys. B* **85**, 73–77 (2006).
- [6] A. Galvanauskas, M. Arbore, M. Fejer, M. Fermann, and D. Harter, *Opt. Lett.* **22**, 105 (1997).
- [7] P. D. Trapani, A. Andreoni, C. Solcia, P. Foggi, R. Danielius, A. Dubietis, and A. Piskarskas, *J. Opt. Soc. Am. B* **12**, 2237 (1995), URL <http://josab.osa.org/abstract.cfm?URI=josab-12-11-2237>.
- [8] J. Fan, W. Chen, C. Gu, Y. Song, L. Chai, C. Wang, and M. Hu, *Opt. Express* **25**, 24594 (2017), URL <http://www.opticsexpress.org/abstract.cfm?URI=oe-25-20-24594>.
- [9] S. Marchese, E. Innerhofer, R. Paschotta, S. Kurimura, K. Kitamura, G. Arisholm, and U. Keller, *Applied Physics B* **81**, 1049 (2005), URL <https://doi.org/10.1007/s00340-005-1964-5>.
- [10] T. Südmeyer, F. Brunner, R. Paschotta, T. Usami, H. Ito, M. Nakamura, K. Kitamura, and U. Keller, in *Conference on Lasers and Electro-Optics* (Optical Society of America, 2002), p. CTuO4, URL <http://www.osapublishing.org/abstract.cfm?URI=CLEO-2002-CTuO4>.
- [11] C. Manzoni, G. Cirri, D. Brida, S. De Silvestri, and G. Cerullo, *Phys. Rev. A* **79**, 033818 (2009), URL <https://link.aps.org/doi/10.1103/PhysRevA.79.033818>.
- [12] H. Linnenbank and S. Linden, *Opt. Express* **22**, 18072 (2014), URL <http://www.opticsexpress.org/abstract.cfm?URI=oe-22-15-18072>.
- [13] H. Linnenbank, T. Steinle, and H. Giessen, *Opt. Express* **24**, 19558 (2016), URL <http://www.opticsexpress.org/abstract.cfm?URI=oe-24-17-19558>.
- [14] P. Zhao, B. Zhang, E. Li, R. Zhou, D. Xu, Y. Lu, T. Zhang, F. Ji, X. Zhu, P. Wang, et al., *Opt. Express* **14**, 7224 (2006), URL <http://www.opticsexpress.org/abstract.cfm?URI=oe-14-16-7224>.
- [15] S. C. Kumar, M. Jelínek, M. Baudisch, K. T. Zawilski, P. G. Schunemann, V. Kubeček, J. Biegert, and M. Ebrahim-Zadeh, *Opt. Express* **20**, 15703 (2012), URL <http://www.opticsexpress.org/abstract.cfm?URI=oe-20-14-15703>.
- [16] O. Chalus, P. G. Schunemann, K. T. Zawilski, J. Biegert, and M. Ebrahim-Zadeh, *Opt. Lett.* **35**, 4142 (2010), URL <http://ol.osa.org/abstract.cfm?URI=ol-35-24-4142>.
- [17] L. Xu, H.-Y. Chan, S. u. Alam, D. J. Richardson, and D. P. Shepherd, *Opt. Express* **23**, 12613 (2015), URL <http://www.opticsexpress.org/abstract.cfm?URI=oe-23-10-12613>.
- [18] A. Aadhi and G. K. Samanta, *Opt. Lett.* **42**, 2886 (2017), URL <http://ol.osa.org/abstract.cfm?URI=ol-42-15-2886>.
- [19] R. Piccoli, F. Pirzio, A. Agnesi, V. Badikov, D. Badikov, G. Marchev, V. Panyutin, and V. Petrov, *Opt. Lett.* **39**, 4895 (2014), URL <http://ol.osa.org/abstract.cfm?URI=ol-39-16-4895>.
- [20] C. Wang, C. Langrock, A. Marandi, M. Jankowski, M. Zhang, B. Desiatov, M. M. Fejer, and M. Lončar, *Optica* **5**, 1438 (2018), URL <http://www.osapublishing.org/optica/abstract.cfm?URI=optica-5-11-1438>.
- [21] M. Jankowski, C. Langrock, B. Desiatov, A. Marandi, C. Wang, M. Zhang, C. R. Phillips, M. Lončar, and M. M. Fejer, *Optica* **7**, 40 (2020), URL <http://www.osapublishing.org/optica/abstract.cfm?URI=optica-7-1-40>.
- [22] D. D. Crouch, *Physical Review A* **38**, 508 (1988), URL <https://doi.org/10.1103/physreva.38.508>.
- [23] A. Boes, L. Chang, M. Knoerzer, T. G. Nguyen, J. D. Peters, J. E. Bowers, and A. Mitchell, *Opt. Express* **27**, 23919 (2019), URL <http://www.opticsexpress.org/abstract.cfm?URI=oe-27-17-23919>.
- [24] J. R. Schwesyg, C. R. Phillips, K. Ioakeimidi, M. C. C.



- Kajiyama, M. Falk, D. H. Jundt, K. Buse, and M. M. Fejer, *Opt. Lett.* **35**, 1070 (2010), URL <http://ol.osa.org/abstract.cfm?URI=ol-35-7-1070>.
- [25] C. R. Phillips, C. Langrock, J. S. Pelc, M. M. Fejer, I. Hartl, and M. E. Fermann, *Opt. Express* **19**, 18754 (2011), URL <http://www.opticsexpress.org/abstract.cfm?URI=oe-19-20-18754>.
- [26] T. P. McKenna, J. D. Witmer, R. N. Patel, W. Jiang, R. V. Laer, P. Arrangoiz-Arriola, E. A. Wollack, J. F. Herrmann, and A. H. Safavi-Naeini, *Optica* **7**, 1737 (2020), URL <http://www.osapublishing.org/optica/abstract.cfm?URI=optica-7-12-1737>.
- [27] H. H. Lim, S. Kurimura, and N. E. Yu, *Opt. Express* **22**, 5209 (2014), URL <http://www.opticsexpress.org/abstract.cfm?URI=oe-22-5-5209>.
- [28] C. Hu, A. Pan, T. Li, X. Wang, Y. Liu, S. Tao, C. Zeng, and J. Xia, *Opt. Express* **29**, 5397 (2021), URL <http://www.opticsexpress.org/abstract.cfm?URI=oe-29-4-5397>.
- [29] J. Hult, *J. Lightwave Technol.* **25**, 3770 (2007), URL <http://jlt.osa.org/abstract.cfm?URI=jlt-25-12-3770>.
- [30] A. Fallahkhair, K. S. Li, and T. E. Murphy, *J. Lightwave Technol.* **26**, 1423 (2008), URL <http://jlt.osa.org/abstract.cfm?URI=jlt-26-11-1423>.

## METHODS

**Experimental details** To characterize the gain and conversion efficiency of OPG in the waveguide, as well as pump depletion, we monitor three powers at the output of the waveguide: the generated signal, the pump, and the green light from the SHG of the pump. We measure the generated signal using an extended InGaAs photoreceiver (NewFocus Model 2034) with a wavelength sensitivity range of 800 – 2200 nm. We use a lock-in amplifier (SRS SR830) to monitor the detected signal. An additional longpass filter (Thorlabs FELH1350) is placed before the photoreceiver to remove any contribution of the transmitted pump from reaching the detector. The characterization of the transmitted pump power and the parasitic green is done with a silicon photodiode (Thorlabs S130C) using a longpass filter (Thorlabs FELH900) to measure the pump and a bandpass filter (Thorlabs FGS900-A) for the green light. All the measured data are compensated for the coupling efficiency into the waveguide, estimated to be between 1 and 2%, and the collection efficiency from the waveguide, estimated to be 30%. Similarly, we characterize the spectrum of the pump and signal by collecting the light output from the waveguide into a zirconium fluoride fiber (Thorlabs P1-23Z-FC-5) and sending the signal to an optical spectrum analyzer. We used a Yokagawa AQ6376 with a span of 1500-3400 nm for the down-converted signal and a Yokagawa AQ6370C with span of 800-1500 nm for the pump.

We note here that given the exponential scaling of the power gain with the incoupled pump power, the generated signal is extremely sensitive to misalignments between the waveguide and the incident pump. We observe

drifts in the measured signal power of 1-3 dB that we attribute to slow temperature drifts of  $\pm 0.1$  C of the crystal mount, which misaligns the waveguide relative to the pump beam. To the greatest extent possible, the output power and generated spectra presented here are taken at the peak signal output power of these drifts. A reduction of the alignment sensitivity can be obtained using tapered edged couplers, which both increase the coupling efficiency into the waveguide and reduce the sensitivity of the system to misalignment [28].

**Determining the phase-mismatch** The estimation of the phase-mismatch is done in two steps. First we measured the SHG of a pump at 2  $\mu\text{m}$  to locate the combination of poling period and temperature that exhibited phase-matched SHG. Then, we can use the known tuning of the phase-mismatch with respect to temperature and poling period to determine the phase-mismatch of adjacent waveguides as a function of temperature. We chose a shift of poling period of 10 nm between adjacent devices, or a  $\Delta kL$  shift by  $4\pi$ . We note here, however, that in the presence of second- and higher-order dispersion, the propagation constant of a short pulse is effectively shifted by a Guoy phase. As an example, for a Gaussian pulse with an envelope given by  $\exp(-t^2/\tau^2)$  the propagation constant is effectively shifted by  $k''/\tau^2$ . The pulse envelopes for SHG and OPG exhibit different shapes and bandwidths, and therefore exhibit slightly different effective phase-shifts due to the Guoy phase on the order of 100's of  $\text{mm}^{-1}$ . For these reasons, we deduce that we operated the experiment with a phase-mismatch of 1.5-2  $\text{mm}^{-1}$ .

**Theory of quasi-static OPG** The evolution of the pump and signal envelopes in a frame moving with the group velocity of the signal are given by the coupled-wave equations (CWEs)

$$\partial_z A_\omega(z, t) = -i\kappa A_{2\omega}(z, t) A_\omega^*(z, t) \exp(-i\Delta k z) \quad (2a)$$

$$+ \hat{D}_\omega A_\omega(z, t),$$

$$\partial_z A_{2\omega}(z, t) = -i\kappa A_\omega^2(z, t) \exp(i\Delta k z) \quad (2b)$$

$$- \Delta k' \partial_t A_{2\omega}(z, t) + \hat{D}_{2\omega} A_{2\omega}(z, t),$$

where  $A_\omega$  is the complex field amplitude of the signal generated around frequency  $\omega$ , normalized such that  $P_\omega = |A_\omega|^2$  corresponds to the instantaneous intensity of the signal centered around  $\omega$ .  $\Delta k' = k'_{2\omega} - k'_\omega$  is the group velocity mismatch between the pump and the generated signal. The dispersion operator  $\hat{D}_\omega = \sum_{j=2}^{\infty} \left( (-i)^{j+1} k_\omega^{(j)} / j! \right) \partial_t^j$  contains contributions from second- and higher-order dispersion, where  $k_\omega^{(j)}$  represents the  $j^{\text{th}}$  derivative of propagation constant  $k$  at frequency  $\omega$ . The nonlinear coupling is given by

$$\kappa = \frac{\sqrt{2Z_0}\omega d_{\text{eff}}}{cn_\omega \sqrt{n_{2\omega} A_{\text{eff}}}}, \quad (3)$$

where  $Z_0$  is the impedance of free space,  $n_\omega$  is the effective index of the relevant mode at frequency  $\omega$ ,

$d_{\text{eff}} = 2d_{33}/\pi$  is the effective nonlinear coefficient ( $d_{33} = 20.5$  pm/V for doubling of 2- $\mu\text{m}$  light), and  $A_{\text{eff}} \approx 1 \mu\text{m}^2$  is the effective area of the nonlinear interaction.

The dominant dispersion orders are  $\Delta k'$ , which limits the pump bandwidth available for parametric down-conversion, and  $k''$ , which limits the bandwidth of the generated signal. In quasi-static devices, where both of these dispersion orders are simultaneously negligible, we may obtain approximate solutions to the CWEs by neglecting dispersion to all orders. In the absence of any dispersion, the CWEs in the time domain are given by

$$\partial_z A_\omega(z, t) = -i\kappa A_{2\omega}(z, t) A_\omega^*(z, t) \exp(-i\Delta k z) \quad (4a)$$

$$\partial_z A_{2\omega}(z, t) = -i\kappa A_\omega^2(z, t) \exp(i\Delta k z). \quad (4b)$$

For an undepleted pump, the evolution of the generated signal envelope  $A_\omega(z, t)$  is given by

$$\begin{aligned} \tilde{A}_\omega = & A_\omega(0, t) \cosh(g(t)z) \\ & + \left( \frac{\gamma(t)}{g(t)} A_\omega^*(0, t) - \frac{i\Delta k}{2g(t)} A_\omega(0, t) \right) \sinh(g(t)z), \end{aligned} \quad (5a)$$

where  $\tilde{A}_\omega \exp(i\Delta k z/2) = A_\omega$ , the instantaneous field gain coefficient is given by  $g(t) = \sqrt{|\gamma|^2(t) - (\Delta k/2)^2}$ , and  $\gamma(t) = -i\kappa A_{2\omega}(0, t)$  is assumed to be real for all  $t$ . We note here that we assume  $A_{2\omega}(0, t)$  is centered around  $t = 0$ , such that  $\gamma_{\text{pk}} = \gamma(0)$ .

The real and imaginary components of  $\tilde{A}_\omega$  are given by  $\tilde{x} = (\tilde{A}_\omega + \tilde{A}_\omega^*)/2$  and  $\tilde{y} = (\tilde{A}_\omega - \tilde{A}_\omega^*)/(2i)$ , respectively. In the limit of large gain, the real part of  $\tilde{A}_\omega$  grows exponentially,

$$\begin{aligned} \tilde{x}_\omega = & x(0, t) \left( \cosh(g(t)z) + \frac{\gamma(t)}{g(t)} \sinh(g(t)z) \right) \\ & + y(0, t) \frac{\Delta k}{2g(t)} \sinh(g(t)z). \end{aligned} \quad (6a)$$

From this approach we find two key insights. First, we note that for large gain the generated signal bandwidth is bounded below by the pump bandwidth since the temporal extent of the amplified signal envelope is smaller than that of the pump. Second, we note that the gain coefficient experienced by the generated signal is comparable to the peak gain of the pump  $\gamma_{\text{pk}}$  since the generated signal is confined to a small temporal window around the peak of the pump. As an example, for a CW seed  $x(0)$  the amplified signal is given by  $\tilde{x}_\omega = x(0) \exp(g(t)z)$ . For intermediate parametric gains, the duration of the amplified signal pulse is given by  $\tau_\omega(z) = \tau/\sqrt{\gamma_{\text{pk}} z}$ . We note here that in the limit of large parametric gain  $\tau_\omega$  does not asymptote to zero. Instead,  $\tau_\omega$  is bounded by the transform limit of the generated OPA bandwidth.

In the absence of pump depletion we may obtain a more complete solution to Eqn. 5a that accounts for the dispersion orders neglected in Eqns 4a-4b by considering the evolution of generated signal in the frequency domain. In the undepleted limit, the evolution of a signal

generated at frequency  $\omega + \Omega'$  is given by

$$\begin{aligned} \partial_z \hat{A}_\omega(z, \Omega') = & -i\kappa \int \hat{A}_{2\omega}(0, \Omega) \hat{A}_\omega^*(z, \Omega - \Omega') \\ & \exp(-i\Delta k(\Omega, \Omega')z) d\Omega, \end{aligned} \quad (7a)$$

where  $\Omega$  parameterizes the frequency detuning within the pump envelope, and  $\Delta k(\Omega, \Omega') = k(2\omega + \Omega) - k(\omega + \Omega') - k(\omega + \Omega - \Omega')$  is the phase-mismatch between the pump and the generated signal and idler waves. We note here that the input pump bandwidth is limited by the transform-limited duration of the pump pulses input to the waveguide and therefore the limits of integration in Eqn. 7a can be truncated at a characteristic frequency  $\pm \Delta\Omega_p$ . The series expansion of  $\Delta k(\Omega, \Omega')$  to second order in  $\Omega$  and  $\Omega'$  is given by,

$$\begin{aligned} \Delta k(\Omega, \Omega') \approx & \Delta k_0 + \Delta k' \Omega \\ & + \frac{k''_{2\omega} - k''_\omega}{2} \Omega^2 - k''_\omega (\Omega'^2 - \Omega\Omega'). \end{aligned} \quad (8a)$$

We again find that the phase-mismatch is dominated to leading order in  $\Omega$  and  $\Omega'$  by  $\Delta k'$  and  $k''_\omega$ , respectively. For broadband OPA, the  $\Omega\Omega'$  term in 8a can be neglected since the range of generated  $\Omega'$  is typically much larger than  $\Delta\Omega_p$ .

Quasi-static operation occurs when these two leading contributions to the phase-mismatch are made to be negligible. In this limit, a number of assumptions can be made to simplify Eqn. 7a. First, we assume that the bandwidth of the generated signal is sufficiently large compared to  $\Delta\Omega_p$  that the contribution of the generated idler to the phase-mismatch can be approximated as  $k(\omega + \Omega - \Omega') \approx k(\omega - \Omega')$ , which renders  $\exp(-i\Delta k(\Omega, \Omega')z) \approx \exp(-i\Delta k_{2\omega}(\Omega)z) \exp(-i\Delta k_\omega(\Omega')z)$ , a separable function of  $\Omega$  and  $\Omega'$ . Here  $\Delta k_\omega(\Omega') = \Delta k(\Omega = 0, \Omega')$  is an even function of  $\Omega'$  and is given to fourth order in  $\Omega'$  by  $\Delta k_\omega(\Omega') \approx \Delta k_\omega(0) + k''_\omega(\Omega')^2/2 + k^{(4)}_\omega(\Omega')^4/24 + \mathcal{O}(\Omega'^6)$ . With these simplifications, Eqn. 7a becomes

$$\begin{aligned} \partial_z \hat{A}_\omega(z, \Omega') = & -i\kappa \exp(-i\Delta k_\omega(\Omega')z) \\ & \int \hat{A}_{2\omega}(z, \Omega) \hat{A}_\omega^*(z, \Omega - \Omega') d\Omega. \end{aligned} \quad (9a)$$

The field envelope of the linearly propagating pump is given by  $\hat{A}_{2\omega}(z, \Omega) = \hat{A}_{2\omega}(0, \Omega) \exp(-ik''_{2\omega}\Omega^2 z/2)$ . For the devices considered here the chirp accumulated by the pump pulses over the length of the device is negligible ( $k''_{2\omega} L \Delta\Omega_p^2/2 \ll \pi$ ). Therefore the pump envelope is essentially unchanged during propagation,  $\hat{A}_{2\omega}(z, \Omega) \approx \hat{A}_{2\omega}(0, \Omega)$ . We note here that in the integral in Eqn. 9a is simply the Fourier transform of Eqn. 4a and can be readily calculated using the time-domain field envelopes.

We may further simplify Eqn. 7a by introducing the effective gain coefficient,

$$\gamma_{\text{eff}}(z, \Omega') = -i\kappa \int \hat{A}_{2\omega}(0, \Omega) \frac{\hat{A}_\omega^*(z, \Omega - \Omega')}{\hat{A}_\omega^*(z, -\Omega')} d\Omega. \quad (10)$$

The second simplifying assumption we make for quasi-static devices is that the shape of the amplified signal is preserved during propagation  $\hat{A}_\omega(z, \Omega') = A(z)f(\Omega')$ . In this case, the effective gain coefficient becomes invariant with respect to  $z$ ,  $\gamma_{\text{eff}}(z, \Omega') = \gamma_{\text{eff}}(0, \Omega')$ . When the generated signal bandwidth is much larger than  $\Delta\Omega_p$  the idler envelope  $\hat{A}_\omega(z, \Omega - \Omega')$  varies slowly with respect to pump detuning  $\hat{A}_\omega(z, \Omega - \Omega') \approx \hat{A}_\omega(z, -\Omega')$ , and the effective gain coefficient simplifies to  $\gamma_{\text{eff}} = -i\kappa \int \hat{A}_{2\omega}(0, \Omega)d\Omega = \gamma_{\text{pk}}$ .

With this definition of the effective gain, Eqn. 7a reduces to the familiar CWEs for non-degenerate OPA with a continuous-wave pump,

$$\begin{bmatrix} \tilde{A}_\omega(z, \Omega') \\ \tilde{A}_\omega^*(z, -\Omega') \end{bmatrix} = \begin{bmatrix} \mu(\Omega') & \nu(\Omega') \\ \nu^*(-\Omega') & \mu^*(-\Omega') \end{bmatrix} \begin{bmatrix} A_\omega(0, \Omega') \\ A_\omega^*(0, -\Omega') \end{bmatrix}, \quad (11a)$$

$$\mu(z, \Omega') = \cosh(\tilde{g}(\Omega')z) + \frac{i\Delta k_\omega(\Omega')}{2\tilde{g}(\Omega')} \sinh(\tilde{g}(\Omega')z) \quad (11b)$$

$$\nu(z, \Omega') = \frac{\gamma_{\text{eff}}(\Omega')}{\tilde{g}(\Omega')} \sinh(\tilde{g}(\Omega')z), \quad (11c)$$

where  $\tilde{A}_\omega(z, \Omega') = A_\omega(z, \Omega') \exp(i\Delta k_\omega(\Omega')z/2)$ , and the frequency dependent field gain coefficient is given by  $\tilde{g}(\Omega') = \sqrt{\gamma_{\text{eff}}(\Omega')\gamma_{\text{eff}}^*(-\Omega') - (\Delta k_\omega(\Omega')/2)^2}$ . It can be shown that the maximum attainable power gain is given by [22]

$$G = \left( \sqrt{\mu(\Omega')\mu^*(-\Omega')} + \sqrt{\nu(\Omega')\nu^*(-\Omega')} \right)^2, \quad (12)$$

or  $G \approx \exp(2\tilde{g}(\Omega')z)$  in the limit of large gain ( $\gamma_{\text{eff}}(\Omega')\gamma_{\text{eff}}^*(-\Omega') \gg (\Delta k/2)^2$ ). Equation 12 is plotted in Fig. 2d as a function of generated signal wavelength and phase-mismatch  $\Delta k(\Omega = 0, \Omega' = 0)$ , with  $\gamma_{\text{eff}} \approx \gamma_{\text{pk}}$  for the effective gain. We note here that for a given phase-mismatch,  $G(\Omega')$  is essentially flat across the range of generated signal frequencies. We therefore expect the generated pulse energy to grow as  $G = \exp(b\sqrt{U_{\text{in}}}) \approx \exp(2\tilde{g}(0)z)$ , with the power gain coefficient  $b$  in dB/ $\sqrt{\text{pJ}}$  determined to good approximation by the peak gain associated with the pump  $\gamma_{\text{pk}}$  and the phase-mismatch of a degenerate signal at  $\omega$ .

For OPG, the seed is given by vacuum fluctuations. The treatment used here is readily extended to the field creation and annihilation operators  $\hat{a}_{\omega,j}^\dagger$  and  $\hat{a}_{\omega,j}$  for a mode at frequency  $\omega_j = \omega + \Omega'_j$ , where  $\Omega'_j = 2\pi j f_R$  and  $f_R$  is the repetition rate of the pump laser. In this case, we have

$$\begin{bmatrix} \hat{a}_{\omega,j}(z) \\ \hat{a}_{\omega,-j}^\dagger(z) \end{bmatrix} = \begin{bmatrix} \mu(\Omega'_j) & \nu(\Omega'_j) \\ \nu^*(-\Omega'_j) & \mu^*(-\Omega'_j) \end{bmatrix} \begin{bmatrix} \hat{a}_{\omega,j}(0) \\ \hat{a}_{\omega,-j}^\dagger(0) \end{bmatrix}, \quad (13)$$

where  $\mu$  and  $\nu$  have the same form as in Eqns 11b-11c. The photon number in mode  $j$  is given by  $\langle 0 | \hat{a}_{\omega,j}^\dagger \hat{a}_{\omega,j} | 0 \rangle = |\nu(\Omega'_j)|^2$ . For a broadband signal, the power contributed

by mode  $j$  is therefore given by

$$P_j(z) = \hbar\omega_j f_R \gamma_{\text{pk}}^2 z^2 \left| \frac{\sinh(g(\Omega'_j)z)}{g(\Omega'_j)z} \right|^2. \quad (14)$$

In the limit of low gain, Eqn. 14 reduces to the familiar power per mode produced by spontaneous parametric down-conversion  $P_j(z) = \hbar\omega_j f_R \gamma_{\text{pk}}^2 z^2 \text{sinc}^2(\Delta k z/2)$ . For a phase-mismatch dominated by fourth-order dispersion,  $g(\Omega'_j)$  is essentially flat until  $\Omega'$  reaches the characteristic bandwidth for OPA  $(\Delta\Omega'_{\text{OPA}})^4 \approx 48\gamma_{\text{pk}}/k_\omega^{(4)}$ . The generated bandwidth is therefore a weak function of pump power, and the total power is given by

$$P(z) = \sum_j P_j \approx 4P_0 |\sinh^2(g(0)z)|^2 N_{\text{OPA}}, \quad (15)$$

where the prefactor is given by  $P_0 = \hbar\omega f_R/4$ , and the number of OPA modes is given by  $N_{\text{OPA}} = \Delta\Omega_{\text{OPA}}/(2\pi f_R)$ . We note here that Eqn. 15 is essentially the power generated by a CW-pumped OPG with an unsaturated gain coefficient  $\gamma_{\text{pk}}$ . For pulsed OPG we need to correct the generated power by the duty cycle,  $\tau_\omega f_R \approx N_{\text{OPA}}^{-1}$ , where the latter form is valid for large gain. We therefore expect a total generated power of

$$P_{\text{out}}(z) = P_0 \exp(2g(0)z). \quad (16)$$

The simple scaling of the detected signal power as a function of pulse energy input to the waveguide allows the gain coefficient  $g(0)$  to be determined directly from  $P_{\text{out}}$  using a simultaneous fit of  $P_0$  and  $g(0)$ . Deviations between the fitted value for  $P_0$  and  $\hbar\omega f_R/4$  can occur due to filtering of the generated bandwidth by the responsivity of the photoreceiver  $R(\omega)$  used to detect the generated light  $P_{\text{det}} = \sum_j P_j R(\omega_j)$ .

**Measuring the gain coefficient and saturated gain using OPG** To estimate the gain coefficient in the undepleted limit, we fitted Eqn. 15 to the generated power for pump pulse energies between 500 fJ and 4 pJ (Fig. 3b, solid black line). This range of pulse energies is chosen both to suppress the effects of pump depletion at high power and reductions in the parametric gain due to phase-mismatch at low power. To compute the saturated gain we simply find the pump pulse energy that would yield the same 200  $\mu\text{W}$  of output power from the unsaturated gain curve as observed in the experiment (Fig. 3b, dashed black line). These curves cross at 6.19 pJ, which corresponds to 88 dB of saturated gain for the measured 35.5 dB/ $\sqrt{\text{pJ}}$  scaling of unsaturated gain with pump pulse energy.

**Simulations** The quasi-static model for OPG presented here is only valid for an undepleted pump and cannot account for either the pump depletion due to conversion to the signal or the pump depletion due to parasitic SHG. Furthermore, the unsaturated gain determined here cannot account for the observed broadening of the signal due to pump depletion. We model these



effects numerically using a three-envelope approach [25], with the evolution of each harmonic given by

$$\partial_z A_1 = -i\kappa_{2,1} A_2 A_1^* \exp(-i\Delta k_{2,1} z) + \hat{D}_1 A_1, \quad (17a)$$

$$\begin{aligned} \partial_z A_2 = & -i\kappa_{2,1} A_1^2 \exp(i\Delta k_{2,1} z) - \Delta k'_{2,1} \partial_t A_2 \\ & - i\kappa_{3,2} A_2 A_3^* \exp(-i\Delta k_{3,2} z) + \hat{D}_2 A_2, \end{aligned} \quad (17b)$$

$$\begin{aligned} \partial_z A_3 = & -i\kappa_{3,2} A_2^2 \exp(i\Delta k_{3,2} z) \\ & - \Delta k'_{3,1} \partial_t A_3 + \hat{D}_3 A_3 - \alpha_3 A_3, \end{aligned} \quad (17c)$$

where the subscript  $j$  refers to the envelope centered around  $\omega_j = 2^{j-1}\omega$ , e.g.  $A_2$  is the pump at  $2\omega$ , and  $A_3$  is the parasitic SHG of the pump at  $4\omega$ .  $\kappa_{j,i}$  is the nonlinear coupling between  $A_i$  and  $A_j$ . The green light formed due to parasitic SHG is observed to scatter out of the waveguide, and therefore includes a loss term  $\alpha$ . Eqns 17a-17c can include self- and cross-phase modulation terms due to  $\chi^{(3)}$  nonlinearities, but these terms were not observed numerically to contribute meaningfully to the nonlinear dynamics for an  $n_2$  of  $3.34 \times 10^{-19} \text{ m}^2/\text{W}$ , and were neglected here. We solve these equations using a split-step Fourier approach, where the step size is chosen using an adaptive Runge-Kutta method (RK4) [29].

The dispersion orders and group velocity mismatch terms can be calculated directly from numerical simulations [30]. The fundamental and second-harmonic include dispersion to fourth order, though the generated power spectra were unchanged when truncating to third order. The dispersion for wavelengths around 500 nm is dominated by a temporal walk-off of 150 fs/mm with respect to the pump, and is truncated to second order. We assume a nonlinear coupling between the generated 2- $\mu\text{m}$  and input 1- $\mu\text{m}$  of  $\kappa_{2,1}^2 = 420 \text{ \%}/\text{W-cm}^2$ , determined by the observed unsaturated gain coefficient of 35.5 dB/ $\sqrt{\text{pJ}}$ . The phase-mismatch between the fundamental and second-harmonic  $\Delta k_{2,1} \approx 1.5 \text{ mm}^{-1}$  is determined using the methods described above.

We note here that the intensity of the green generated in the nonlinear waveguide and the observed spectral broadening is *not* consistent with the calculated nonlinear coupling of  $\kappa_{3,2}^2 = 6800 \text{ \%}/\text{W-cm}^2$ , given by the overlap between the  $\text{TE}_{00}$  modes at 1  $\mu\text{m}$  and 525 nm, and the calculated phase-mismatch  $\Delta k_{3,2} = 300 \text{ mm}^{-1}$ . In practice, cascaded SHG between the pump and parasitic green involves multiple spatial modes and all of the Fourier components associated with the nonlinear grating. The field amplitude generated in the  $n$ th spatial mode of the parasitic green is given by

$$\begin{aligned} \partial_z A_3^{(n)} = & -i \sum_m \kappa_{3,2}^{(m,n)} A_2^2 \exp(i\Delta k_{3,2}^{(m,n)} z) \\ & - \Delta k'_{3,1} \partial_t A_3^{(n)} + \hat{D}_3^{(n)} A_3^{(n)} - \alpha_3 A_3^{(n)}, \end{aligned}$$

where the nonlinear coupling and phase-mismatch associated with the  $m$ th Fourier component of the nonlinear grating are given by  $\kappa_{3,2}^{(m,n)} = \kappa_{3,2}^{(0,n)}/m$  for odd  $m$  and

$\Delta k^{(m,n)} = k_3^{(n)} - 2k_2 - 2\pi m/\Lambda_G$  for a poling period of  $\Lambda_G$ . Similarly, in the limit of large phase-mismatch the effective nonlinear coefficient for self-phase modulation due to back-action of the second harmonic is given by

$$\gamma_{\text{SPM}} = - \sum_{m,n} \frac{\left(\kappa_{3,2}^{(m,n)}\right)^2}{\Delta k_{3,2}^{(m,n)}}. \quad (19)$$

As a proxy for these effects, we take  $\kappa_{3,2}$  and  $\Delta k_{3,2}$  as fitting parameters. The experimentally observed spectral broadening of the pump and the associated pump depletion for large pulse energy is a weak function of poling period and the generated 2- $\mu\text{m}$  signal, and therefore in fitting  $\Delta k_{3,2}$  we set  $\kappa_{2,1} = 0$  to isolate these effects. We find  $\Delta k_{3,2} \approx 60 \text{ mm}^{-1}$ , and  $\kappa_{3,2}^2 = 9800 \text{ \%}/\text{W-cm}^2$  gives qualitative agreement in terms of pump depletion and the generated spectral broadening. All of the dynamics observed here are a weak function of  $\alpha_3$ , and we assume a value of 20 dB/cm.

## ACKNOWLEDGEMENTS

The authors wish to thank NTT Research for their financial and technical support. Electrode patterning and poling was performed at the Stanford Nanofabrication Facility, the Stanford Nano Shared Facilities (NSF award ECCS-2026822), and the Cell Sciences Imaging Facility (NCRR award S10RR02557401). Patterning and dry etching was performed at the Harvard University Center for Nanoscale Systems (CNS), a member of the National Nanotechnology Coordinated Infrastructure (NNCI) supported by the National Science Foundation. The authors acknowledge support from National Science Foundation (NSF) (ECCS-1609688, EFMA-1741651, CCF-1918549); Department of Energy (DoE) (DE-AC02-76SF00515); Army Research Laboratory (ARL) (W911NF-15-2-0060, 48635-Z8401006), and the Swiss National Science Foundation (SNSF-P400P2-194369).

## AUTHOR CONTRIBUTIONS

M.J. and N.J. performed the experiment. M.J. performed theory and design. C.L. and A.M. poled the thin film lithium niobate, and B.D. patterned and etched the waveguides. M.J. and N.J. wrote the manuscript with input from all authors. M.L. and M.M.F. directed the project.

## COMPETING INTERESTS

The authors declare no competing interests.